Int J Earth Sci (Geol Rundsch) (2014) 103:123–140
DOI 10.1007/s00531-013-0959-4

ORIGINAL PAPER

Sr–Nd isotope geochemistry and tectonomagmatic setting of the Dehsalm Cu–Mo porphyry mineralizing intrusives from Lut Block, eastern Iran

R. Arjmandzadeh · J. F. Santos

Received: 28 January 2013 / Accepted: 16 August 2013 / Published online: 29 August 2013

Abstract The Dehsalm Cu–Mo-bearing porphyritic granitoids belong to the Lut Block volcanic–plutonic belt (central eastern Iran). These rocks range in composition from gabbro-diorite to granite, with dominance of monzonites and quartz monzonites, and have geochemical features of high-K calc-alkaline to shoshonitic volcanic arc suites. Primitive mantle-normalized trace element spider diagrams display strong enrichment in large-ion lithophile elements such as Rb, Ba and Cs and depletions in some high-field strength elements, e.g., Nb, Ti, Y and HREE. Chondrite-normalized plots display significant LREE enrichments, high La_N/Yb_N and a lack of Eu anomaly. High Sr/Y and La/Yb ratios of Dehsalm intrusives reveal that, despite their K-rich composition, these granitoids show some resemblances with adakitic rocks. A Rb–Sr whole rock–feldspar–biotite age of 33 ± 1 Ma was obtained in a quartz monzonite sample and coincides, within error, with a previous geochronological result in Chah-Shaljami granitoids, further northwest within the Lut Block. $(^{87}Sr/^{86}Sr)_i$ and εNd_i isotopic ratios range from 0.70481 to 0.70508 and from +1.5 to +2.5, respectively, which fits into a supra-subduction mantle wedge source for the parental melts and indicates that crustal contribution for magma diversification was of limited importance. Sr and Nd isotopic compositions together with major and trace element geochemistry point to an origin of the parental magmas by melting of a metasomatized mantle source, with phlogopite breakdown playing a significant role in the geochemical fingerprints of the parental magmas; small amounts of residual garnet in the mantle source also help to explain some trace element patterns. Geochemical features of Dehsalm porphyries and its association with Cu–Mo mineralization agree with a mature continental arc setting related to the convergence of Afghan and Lut plates during Oligocene.

Keywords Lut Block · High-K calc-alkaline to shoshonitic magmas · Trace element geochemistry · Sr and Nd isotopes · Rb–Sr age · Porphyry deposits

R. Arjmandzadeh (✉)
Department of Geology, Payame Noor University,
P.O. Box No. 19395-3697, Tehran, Islamic Republic of Iran
e-mail: arjmand176@gmail.com

J. F. Santos
Geobiotec Research Unit, Department of Geosciences,
University of Aveiro, 3810-193 Aveiro, Portugal

Introduction

The Lut Block is a geotectonic unit, in eastern Iran, composed of lithologies that, in general, were not significantly affected by tectonic deformation since the Jurassic times. This unit is surrounded by highly deformed domains of clear oceanic affinity, with ophiolite series and flysch-type rocks, particularly to the north, south and east (Stöcklin 1972). The present eastern border of the Lut Block would have belonged to the active margin of the subducted Neotethys Ocean (Dercourt et al. 2000; Golonka 2004; Bagheri and Stampfli 2008). This ocean closed in eastern Iran, between the Afghan and Lut plates, in the Oligocene–Middle Miocene (Sengör and Natalin 1996). The East Iran ophiolite complex marks the boundary between the Lut and Afghan continental blocks (Fig. 1).

The East Iran volcanic–plutonic belt extends for 1,000 km in the N–S direction, within the Lut Block (Figs. 1, 2). The magmatic activity, mainly with calc-alkaline signatures as shown by Berberian (1983), began in the middle Jurassic (165–162 Ma) and reached its peak in

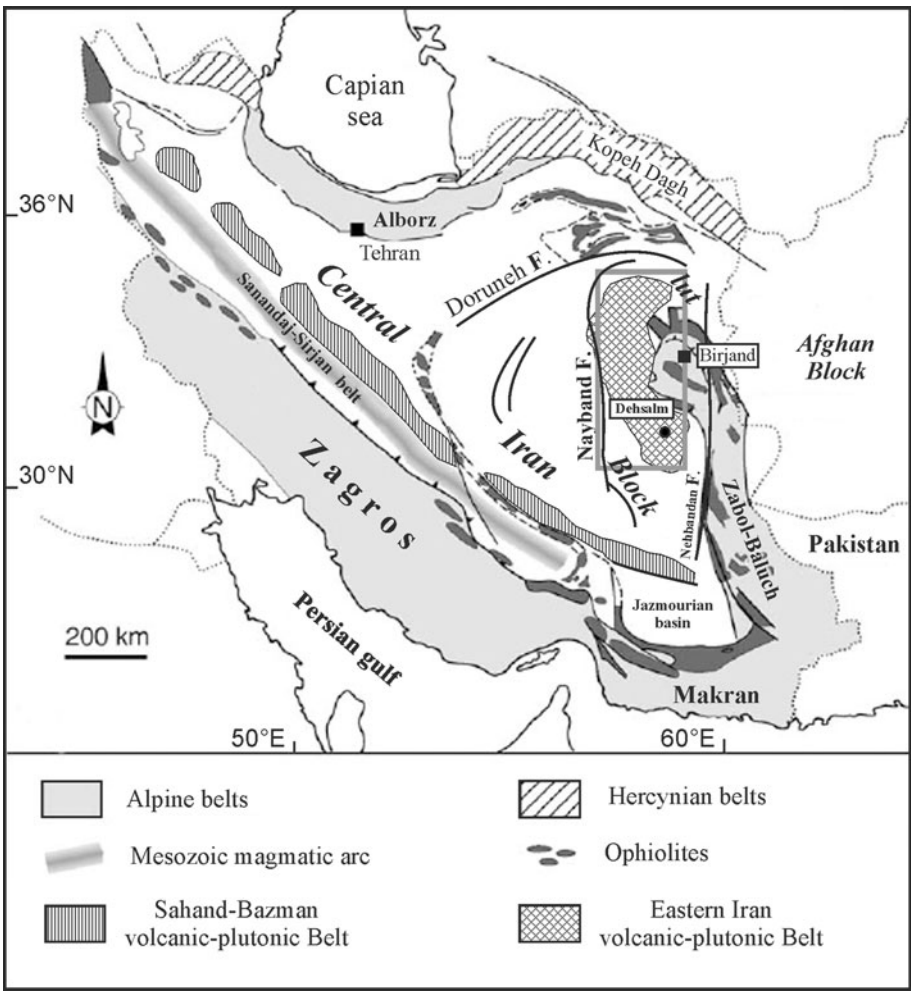

Fig. 1 Modified geological sketch map of Iran after Berberian and King (1981). The *point* indicates the location of Dehsalm intrusives, and the *box* indicates the location of the Lut Block volcanic–plutonic belt

the Tertiary, especially in the middle Eocene. Volcanic and subvolcanic rocks of Tertiary age cover large areas of the Lut Block, attaining a thickness up to 3,000 m, and seem to have resulted from subduction prior to the collision of the Arabian and Eurasian plates (Camp and Griffis 1982; Tirrul et al. 1983; Berberian et al. 1999). According to Eftekharnejad (1981), magmatism in the northern Lut area resulted from subduction beneath the Lut Block. Recently, a two-sided asymmetric subduction model has been proposed to explain the Tertiary magmatic and metallogenic events recorded in the Lut Block (Arjmandzadeh et al. 2011). In this model, west-verging subduction beneath the Lut Block was steeper and faster, favoring the formation of great amounts of calc-alkaline magmas, as recorded within the Lut Block; in contrast, east-verging subduction, under the Afghan block, is testified by stronger tectonic deformation but less important magmatism.

Various mineralization types, such as Cu–Mo–Au porphyry-type deposits, epithermal-type ores, Cu–Au–Ag IOCG-type deposits, Cu and Au–Sb–Pb–Zn vein-type deposits, Cu–Au massive sulfide-type deposits, granite-related Sn–W–Au ores and magmatic-skarn Sn deposits, formed during Jurassic to Tertiary stages of magmatism in the Lut Block (e.g., Malekzadeh 2009; Arjmandzadeh et al. 2011).

The Dehsalm porphyritic granitoids belong to the East Iran volcanic–plutonic belt (Fig. 2) and have associated Cu–Mo porphyry-type deposits (Arjmandzadeh et al. 2013). The purpose of this work is to present and discuss geochemical (both elemental and isotopic) and geochronological (Rb–Sr) data from those shallow intrusives, aiming at establishing tighter constraints on the petrogenetic processes and the geodynamic evolution of the Lut Block.

Geological setting and mineralization

The Lut Block is composed of pre-Jurassic metamorphic rocks and Jurassic sediments, intruded by Jurassic and Tertiary plutons, mainly of granitoids, and covered by Tertiary mafic to felsic lava flows and pyroclastic materials. Magmatism in the Lut Block, represented by a variety of lava

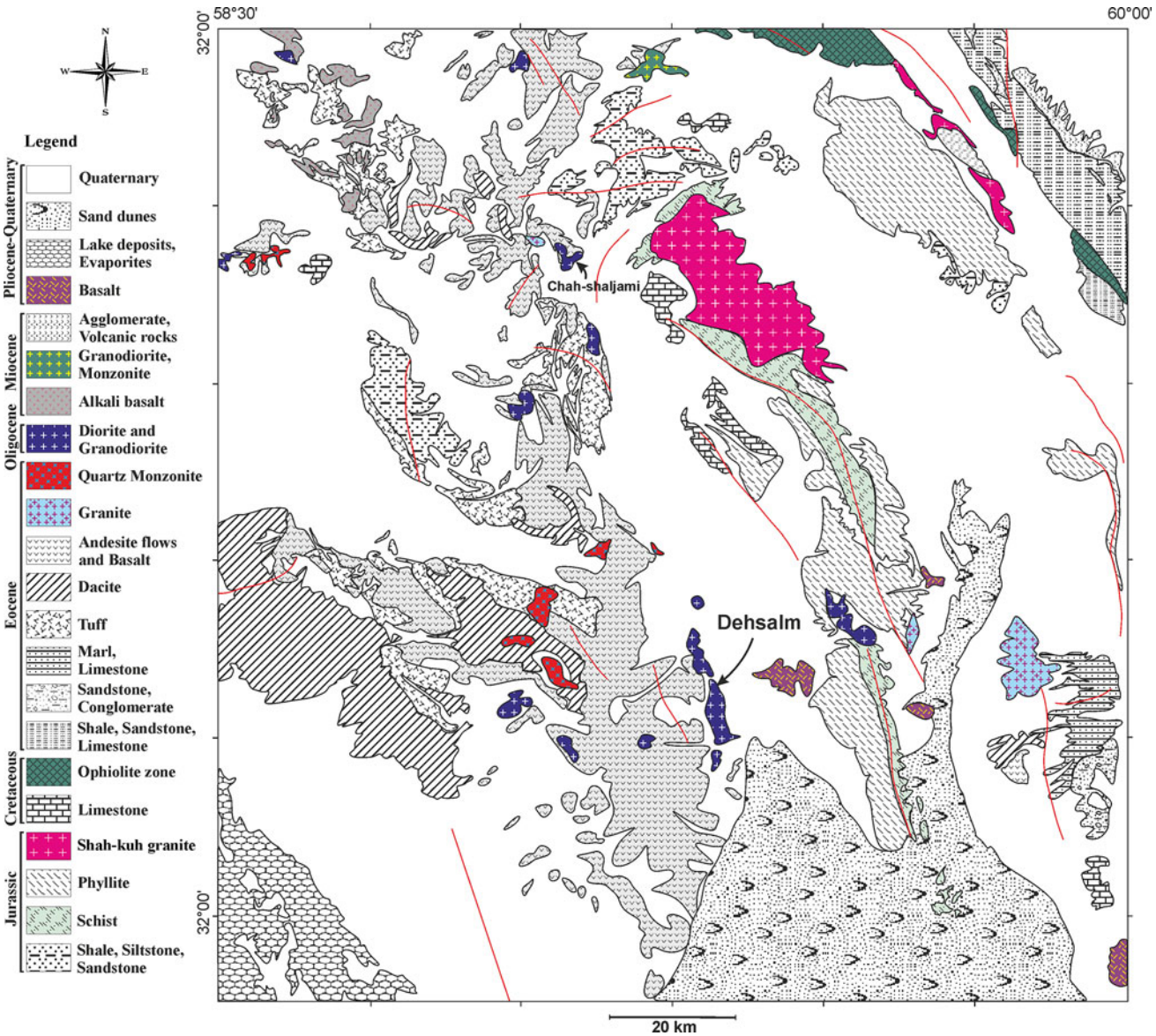

Fig. 2 Geological map of the Lut Block volcanic–plutonic belt and the location of Dehsalm intrusives. Adapted from Griffis et al. (1992)

flows, volcaniclastic rocks and subvolcanic and plutonic bodies, started in the late Jurassic with the intrusion of Shah-Kuh batholith and continued into the Quaternary (Esmaeily 2005). Most of the East Iran mineral deposits are related to the Tertiary magmatism (Arjmandzadeh et al. 2013).

The Dehsalm intrusive complex is located about 55 km west of Nehbandan, in the South Khorasan province. This complex is composed essentially of stocks intrusive into Eocene volcanics, sandstones and siltstones (Fig. 3). The intrusive rocks range from gabbro to granite, with a clear dominance of monzonite and quartz monzonite. Plagioclase is a major rock-forming mineral in most lithologies. K-feldspar is common as phenocrysts as well as in the matrix in the more felsic rock types; it also occurs as a minor phase, interstitial to plagioclase and ferromagnesian minerals in the mafic rocks. Biotite, clinopyroxene and hornblende are the mafic silicates present, in variable proportions, in the studied intrusions (Fig. 4a). Apatite and oxide minerals (magnetite and lesser ilmenite) are common accessory phases, especially in the most mafic rocks.

Most of the felsic-intermediate intrusions display a porphyritic texture, due to the occurrence of millimeter-sized phenocrysts of plagioclase and K-feldspar, surrounded by a groundmass formed by crystals (mainly of feldspars and quartz) no larger than tenths of millimeter. In quartz monzonites, the length of K-feldspar phenocrysts may attain almost 1 cm (Fig. 4b). Plagioclase phenocrysts usually display compositional zoning (Fig. 4c), which is most commonly of the normal type, but, especially in the biggest ones, may also be oscillatory.

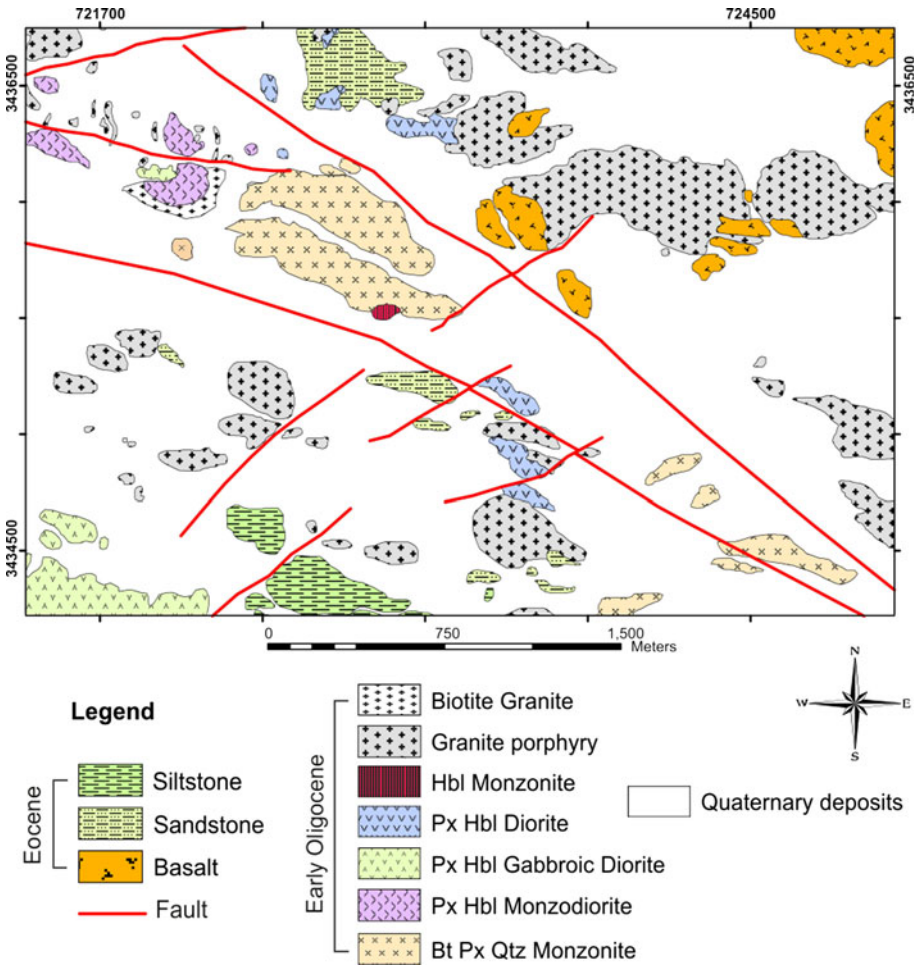

Fig. 3 Geological map of Dehsalm area, after Arjmandzadeh et al. (2013)

A pyroxene-hornblende gabbroic diorite displays a poikilitic texture (Fig. 4d), with large irregular and optically continuous K-feldspar grains hosting several small crystals of other minerals, dominantly plagioclase, hornblende and clinopyroxene.

The diorite usually contains variably oriented subhedral plagioclase laths that define a framework whose interspaces are occupied by small grains of mafic minerals, in an intergranular-like texture. In monzodiorite compositions, K-feldspar becomes a more abundant phase, but systematically with an interstitial character.

Crosscutting relations at surface exposures and in the diamond drill boreholes suggest that quartz monzonite stocks were the earliest, while the biotite granite (as small stocks and dikes) was the latest intrusions emplaced in the Dehsalm complex.

The quartz monzonite stocks have been affected by potassic alteration, represented by abundant secondary biotite. The secondary biotite alteration is overprinted by sericite–calcite–quartz alteration and cut by quartz + pyrite + galena + sphalerite + chalcopyrite veinlets (Fig. 5a). The quartz monzonite also hosts several quartz + pyrite + magnetite + molybdenite + chalcopyrite + anhydrite ± gold veins (Fig. 5b).

Monzonites and diorites show weak or no mineralization potential, despite the fact that propylitization is not uncommon in monzonites.

Granites are variably sericitized and are cut by several types of veins and veinlets: quartz + pyrite + molybdenite; quartz + pyrite + chalcopyrite + arsenopyrite ± gold; and quartz + pyrite + galena + sulfosalts.

Previous studies on alteration, hydrothermal fluids and ore-forming processes indicated the occurrence of a Cu–Mo porphyry-type mineralization in the area (Arjmandzadeh et al. 2013).

Analytical techniques

Major and trace element analysis

After a detailed petrographic study (using transmitted and reflected light microscopy) of a large set of samples collected in various rock units, from both surface exposures

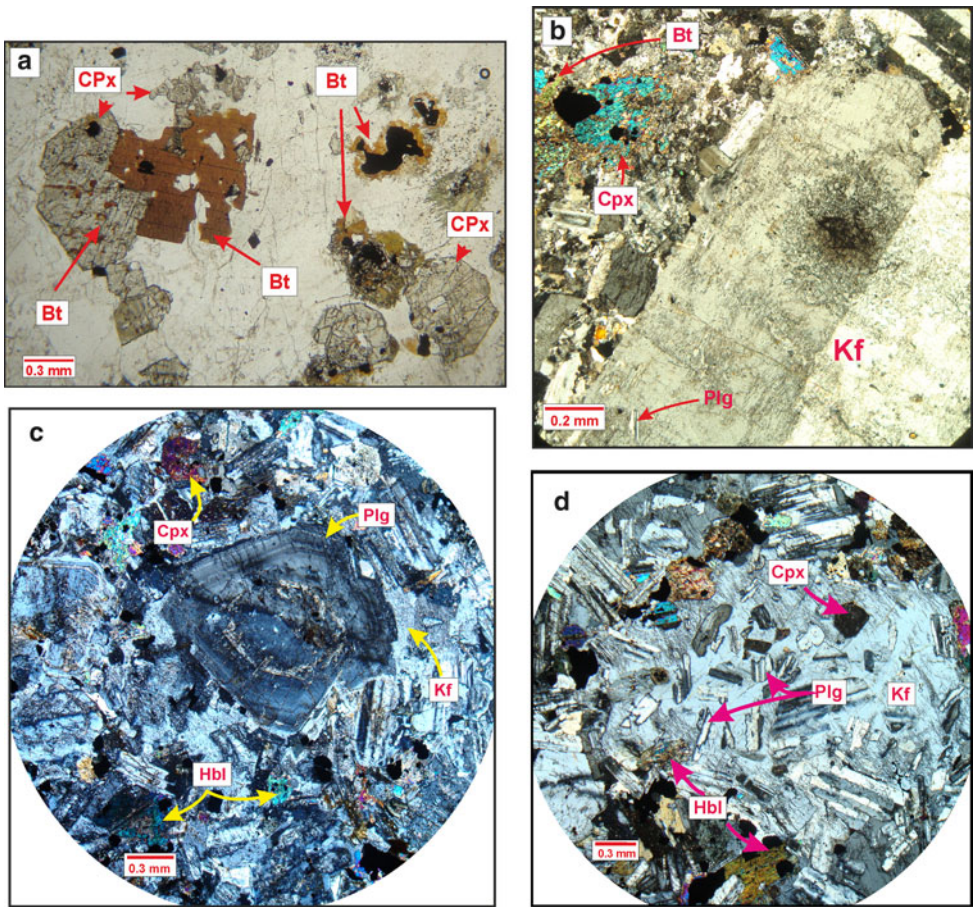

Fig. 4 **a** Late-stage biotite in monzodiorite sample D4-245 (borehole). Besides forming large anhedral grains (that sometimes enclose plagioclase and/or clinopyroxene crystals), biotite also appears as thin rims around the opaque minerals and as patches inside clinopyroxene (PPL-10X). **b** K-feldspar megacrysts in biotite pyroxene quartz monzonite (XPL-10X). **c** Plagioclase showing complex zonation in a pyroxene-hornblende monzodiorite (XPL-10X). **d** Poikilitic texture in pyroxene-hornblende monzonite intrusive body. Pyroxene and plagioclase inclusions distributed throughout the K-feldspar poikilocryst

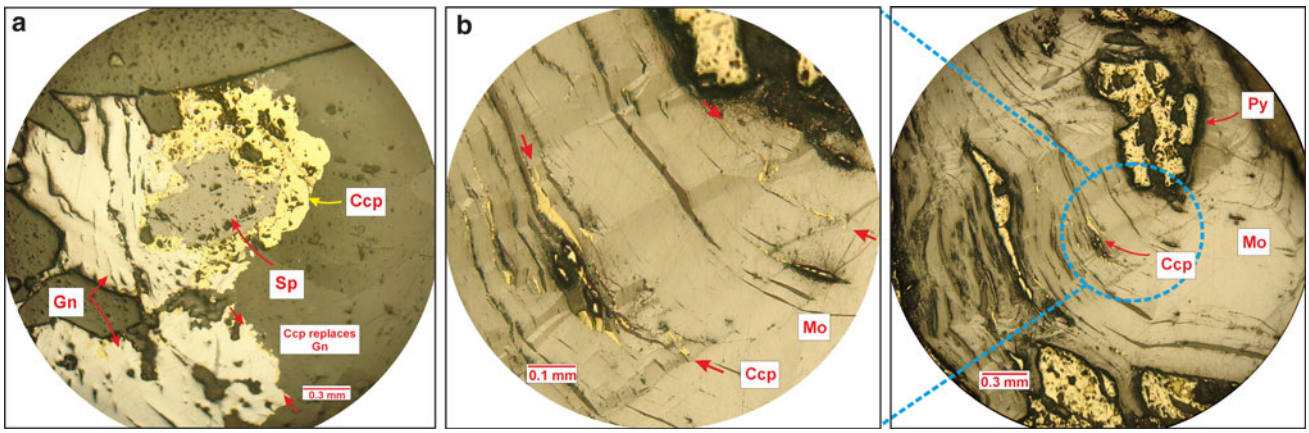

Fig. 5 **a** Galena and sphalerite replaced by chalcopyrite. This setting belongs to the veins including paragenetic minerals such as quartz, pyrite, galena, sphalerite and chalcopyrite, which formed within the sericite–calcite–quartz alteration zone. **b** Molybdenite (Mo), chalcopyrite (Ccp) and pyrite (Py). Chalcopyrite seems to replace the other minerals, mainly through the molybdenite cleavages (PPL-10X). This setting belongs to the veins including paragenetic minerals such as quartz, anhydrite, magnetite, molybdenite, chalcopyrite, pyrite and gold

and drill cores, fourteen of the least altered samples were selected for whole-rock geochemical elemental analysis. The samples were analyzed for major elements by wavelength-dispersive X-ray fluorescence (XRF) spectrometry of fused disks by a Philips PW 1410 XRF spectrometer at Ferdowsi University of Mashhad, Iran. Eleven of these samples were analyzed for trace elements using inductively coupled plasma-mass spectrometry (ICP-MS), following a lithium metaborate/tetraborate fusion and nitric acid total digestion, in the Acme Laboratories, Vancouver (Canada). Whole-rock analytical results for major element oxides and trace elements are listed in Table 1.

Rb–Sr and Sm–Nd isotopic analysis

Sr and Nd isotopic compositions were determined for seven whole-rock samples and two mineral separates (plagioclase and biotite) of the Dehsalm granitoids at the Laboratório de Geologia Isotópica da Universidade de Aveiro, Portugal. Plagioclase and biotite were separated from sample D3-227 using magnetic separation procedures and purified by handpicking under a binocular microscope. The mineral separates were rinsed using double-distilled water and crushed in several steps to remove inclusions and then powdered in agate mortar. The selected powdered samples were dissolved with HF/HNO_3 in Teflon Parr acid digestion bombs at 200 °C for 3 days. After evaporation of the final solution, the samples were dissolved with HCl (6 N) and dried. The target elements were purified using conventional ion chromatography technique in two stages: (1) separation of Sr and REE elements in ion exchange column with AG8 50 W Bio-Rad cation exchange resin and (2) purification of Nd from other lanthanide elements in columns with Ln Resin (ElChrom Technologies) cation exchange resin. All reagents used in the preparation of the samples were sub-boiling distilled, and the water was produced by a Milli-Q Element (Millipore) apparatus. Sr was loaded on a single Ta filament with H_3PO_4, whereas Nd was loaded on a Ta outer-side filament with HCl in a triple-filament arrangement. $^{87}Sr/^{86}Sr$ and $^{143}Nd/^{144}Nd$ isotopic ratios were determined using a Multi-Collector Thermal Ionization Mass Spectrometer (TIMS) VG Sector 54. Data were acquired in dynamic mode with peak measurements at 1–2 V for ^{88}Sr and 0.8–1.5 V for ^{144}Nd. Sr and Nd isotopic ratios were corrected for mass fractionation relative to $^{88}Sr/^{86}Sr = 0.1194$ and $^{146}Nd/^{144}Nd = 0.7219$. During this study, the SRM-987 standard gave an average value of $^{87}Sr/^{86}Sr = 0.710256(16)$ ($N = 12$; conf. lim = 95 %) and $^{143}Nd/^{144}Nd = 0.5121057(61)$ ($N = 13$; conf. lim = 95 %) for the JNdi-1 standard ($^{143}Nd/^{144}Nd$ data are normalized to the La Jolla standard). The concentrations of Rb, Sr, Sm and Nd in the mineral separates and in two whole-rock samples (D3-227 and De-7) were determined by isotope dilution mass spectrometry method (IDMS), using a $^{87}Rb/^{84}Sr$ and $^{150}Nd/^{149}Sm$ double spike. The Rb–Sr and Sm–Nd isotopic compositions are listed in Table 2.

Geochemistry

Major element geochemistry

The Dehsalm intrusive bodies have SiO_2 contents from 52 to 69 wt% and plot mainly in the gabbroic diorite, diorite, monzodiorite, quartz monzonite and granite domains on the Middlemost (1985) diagram (Fig. 6). The samples plot in the fields of high-K calc-alkaline and shoshonitic series on the K_2O versus SiO_2 discrimination diagram proposed by Peccerillo and Taylor (1976) (Fig. 7), showing a strong potassium enrichment (1.57–5.87 K_2O wt%) from the most mafic to the most felsic compositions. Since the Na_2O (2.32–3.65 wt%) trend does not show any obvious correlations with silica enrichment, the K_2O/Na_2O ratios increase from 0.57 to 1.68 toward the more evolved compositions. On the other hand, MgO, FeO_t, CaO, P_2O_5 and TiO_2 decrease with increasing SiO_2 (Fig. 8).

As a whole, the major element variation diagrams point to a differentiation mechanism controlled mostly by fractionation of clinopyroxene, plagioclase and hornblende, in agreement with the order of crystallization that can be inferred from textural criteria. The expected increasing Na contents in fractionating plagioclase with differentiation, precluding a clear Na_2O enrichment in the evolved magmas, can explain the variation of K_2O/Na_2O ratio. Fractionation of apatite, and to some extent oxide minerals (Fe–Ti oxides), should also have played a role in magma differentiation, as testified by the constant and regular decreases in phosphorus, iron and titanium with increasing SiO_2 contents. Similar trends have been reported for several porphyry copper deposits elsewhere (Mason and McDonald 1978; Eastoe and Eadington 1986; Dilles 1987).

The $Al_2O_3/(CaO + Na_2O + K_2O)$ molar ratios are always below 1.1, showing that the Dehsalm intrusions are metaluminous or only slightly peraluminous, as is expected in both M- and I-type granitoids but not in S-type granitoids (White and Chappell 1983; Chappell and White 1992).

The Dehsalm intrusions have MgO contents from 0.92 to 4.6 wt%, and the magnesium numbers (Mg# = 100 * Mg/[Mg + Fe], using atomic proportions) are moderately high, ranging from 40.1 to 55.6.

Trace element geochemistry

Primitive mantle-normalized trace element spider diagrams display strong enrichments in large-ion lithophile elements (LILE) and those incompatible elements that behave similarly to LILE (Th and U) (Fig. 9). The most characteristic high-field strength elements (HFSE)—e.g., Nb, Zr, Y, Ti and HREE—have, compared to LILE, clearly lower normalized values; Nb and Ti, in particular, display negative anomalies (Fig. 9). These features are typical of subduction-related magmas, such as the calc-alkaline volcanic arcs of continental active margins (e.g., Gill 1981; Pearce 1983; Wilson 1989; Walker et al. 2001). High Sr and low Nb, Ta and Ti contents, as in the Dehsalm intrusions, are thought to be due to the absence of plagioclase and presence of Fe–Ti oxides in the residue in the source area of the

Table 1 Whole-rock major and trace element compositions of the studied intrusive rocks of Dehsalm

Sample	de13	D7-93	de-40	de26	D3-227	D6-227	D9-241	de-12	D4-245	de-14	de-8	D12-250	de-7	D10-67
Sample	721865	722761	722380	722901	722596	722291	722850	721908	721793	722028	721766	723150	721634	722550
location	3435956	3435670	3434056	3435550	3436092	3436514	3435950	3436034	3436351	3435803	3436884	3435550	3436835	3435850
Petrography	Bt granite	Bt granite	Px Hbl gabbroic diorite	Hlb monzonite	Px Bt Qtz monzonite	Px Hbl diorite	Px Bt Qtz monzonite	Px Hbl diorite	Px Bt monzodiorite	Bt Px monzonite	Px Hbl diorite	Bt Qtz monzonite	Px Hbl monzodiorite	Bt Qtz monzonite
Wt%														
SiO_2	69.05	66.73	51.99	60.14	61.14	54.09	61.25	57.88	53.12	63.71	54.5	61.35	53.41	61.66
TiO_2	0.33	0.42	0.64	0.46	0.6	0.78	0.56	0.65	0.83	0.43	0.63	0.62	0.71	0.55
Al_2O_3	14.13	14.28	14.8	13.74	15.26	15.01	14.95	14.92	15.06	14	14.25	14.96	14.3	14.13
TFeO	2.45	3.22	7.85	5.79	5.58	6.59	5.54	5.9	7.49	4.51	7.16	5.28	7.3	5.49
MnO	0.02	0.09	0.14	0.18	0.07	0.14	0.11	0.12	0.13	0.09	0.15	0.13	0.13	0.13
MgO	0.92	1.61	4.2	2.47	2.25	4.62	2.21	4.14	3.67	2.79	3.66	2.47	4.14	2.52
CaO	1.26	3.4	10.44	5.19	4.24	10.02	4.98	7.03	8.85	3.36	9.09	5	9.54	4.59
Na_2O	3.14	3.24	2.91	3.65	2.59	2.32	2.53	2.98	2.86	3.62	2.73	2.42	2.57	2.94
K_2O	5.87	4.38	1.57	5.65	5.22	1.64	5.06	2.7	3.04	5.12	2.59	5.1	2.51	4.95
P_2O_5	0.1	0.18	0.45	0.33	0.24	0.5	0.25	0.43	0.62	0.2	0.49	0.24	0.58	0.27
L.O.I	1.15	1.87	4.14	1.68	1.06	2.95	1.79	1.44	2.97	0.85	2.93	2.92	2.87	1.77
ppm														
Ba				1146	834	1059	806	961	1036	886	1284	679	1105	889
Be				3	2	1	2	1	3	3	1	2	<1	2
Co				11.2	12.3	10.3	9.9	18	22.7	9.2	15.5	12.6	22.5	8
Cs				2.6	13.5	2.6	10	3.4	2.8	4.4	3.2	1.6	2.7	13.2
Ga				15.1	16.1	19.2	15.3	18.1	19	15.5	17.8	15.4	17.3	15.9
Hf				7	8.3	4.2	7	6.1	6.9	8	4.3	4.1	3.7	6.1
Nb				30.5	21.5	8.7	20.6	13.1	14.7	21.4	10.2	11.8	9.6	21.5
Rb				146.8	204.7	49	179.3	85.7	80.2	165.9	70.4	115.6	65.6	180.3
Sn				3	2	2	2	2	2	1	1	<1	1	2
Sr				878.2	674.5	1210	647.5	1139	1339	626.2	1445	683.5	1380	674.8
Ta				1.5	1.4	0.4	1.2	0.6	0.6	1.4	0.6	1	0.5	1.3
Th				35.7	42.3	10.8	39.4	19.1	18.5	33	19.9	19.6	12.3	39.3
U				5.5	11.8	2.9	10.9	4.9	4.3	8	5.9	5.5	2.6	11.3
V				84	110	259	102	166	229	72	215	87	224	114
W				2.3	5.2	1.7	2.8	1.3	1.8	3.3	2.2	1.3	1.2	5.6
Zr				239.8	282.9	143.9	261	187.5	254.4	297.6	150.1	133.9	125.7	233.5
Y				18.9	20.3	22.2	20.2	17.9	22.5	19.3	21.8	13	19.1	21.3
La				48.9	57.9	44.7	58	44.8	57.2	57.4	65.1	32.4	50.8	53.5
Ce				105.8	109.2	86.8	108.9	86.2	109.1	108.1	119.9	57.3	98.4	100.5
Pr				11.84	11.67	10.19	11.58	9.61	12.37	11.34	12.79	6.15	10.88	10.92
Nd				42.7	37.9	38.6	38.1	34.7	47.9	39.8	47.1	21.6	41.8	38.6
Sm				7.22	6.34	7.2	6.41	6.14	8.03	6.23	7.79	3.62	7.23	6.35
Eu				1.81	1.35	1.93	1.33	1.61	2.16	1.21	1.99	0.92	2.02	1.34
Gd				5.46	4.61	5.88	4.58	4.57	6.21	4.5	5.71	2.82	5.37	4.6
Tb				0.76	0.68	0.85	0.7	0.69	0.85	0.65	0.82	0.43	0.75	0.71
Dy				3.61	3.6	4.31	3.47	3.36	4.25	3.37	4.02	2.32	3.77	3.75
Ho				0.67	0.68	0.81	0.68	0.62	0.74	0.61	0.73	0.43	0.7	0.68

Table 1 continued

Sample	de13	D7-93	de-40	de26	D3-227	D6-227	D9-241	de-12	D4-245	de-14	de-8	D12-250	de-7	D10-67
Sample location	721865 3435956	722761 3435670	722380 3434056	722901 3435550	722596 3436092	722291 3436514	722850 3435950	721908 3436034	721793 3436351	722028 3435803	721766 3436884	723150 3435550	721634 3436835	722550 3435850
Petrography	Bt granite	Bt granite	Px Hbl gabbroic diorite	Hlb monzonite	Px Bt Qtz monzonite	Px Hbl diorite	Px Bt Qtz monzonite	Px Hbl diorite	Px Bt monzodiorite	Bt Px monzonite	Px Hbl diorite	Bt Qtz monzonite	Px Hbl monzodiorite	Bt Qtz monzonite
Er				1.92	1.94	2.28	2.09	1.81	1.98	1.89	2.19	1.13	1.87	1.86
Tm				0.28	0.3	0.32	0.32	0.25	0.29	0.31	0.32	0.18	0.28	0.31
Yb				1.83	2.05	2.07	2.06	1.6	1.84	1.94	1.94	1.23	1.69	2.01
Lu				0.27	0.31	0.29	0.32	0.24	0.27	0.31	0.3	0.19	0.24	0.32
Eu/Eu*				0.88	0.76	0.91	0.75	0.93	0.94	0.70	0.91	0.88	0.99	0.76
Mg#	40.09	47.12	48.81	43.19	41.81	55.54	40.48	55.56	46.61	52.43	47.62	45.46	50.26	44.99

n.d. means "not determined"

parental magmas (Martin 1999); Nb and Ta impoverishment has also been attributed to earlier depletion events in the mantle source rocks (Woodhead et al. 1993; Gust et al. 1997). In the case of Ti, and taking into account the geochemical and petrographic evidence discussed above, its negative anomalies are also related to the fractionation of oxides. The phosphorus negative anomalies in the studied samples can be explained by fractionation of apatite.

Rare-earth element patterns of the Dehsalm intrusives in chondrite-normalized plots display high degrees of REE fractionation, with strong enrichment in LREE (Fig. 10), as testified by the range of La_N/Yb_N values between 14.5 and 22.6. Their strong resemblance to each other suggests a common magma source and a similar trend of evolution.

Most of the studied rocks have Eu/Eu* ratios from 0.88 to 0.99 (Table 1). Normally, a negative Eu anomaly develops with magma differentiation due to fractional crystallization of early, calcium-rich, plagioclase (Henderson 1984). However, at high fO_2 conditions, Eu will be present mainly as Eu^{3+} and, therefore, only small amounts of Eu^{2+} will be available for incorporation in plagioclase (Drake and Weill 1975). This may be the explanation for the lack of distinct negative Eu anomalies in the Dehsalm intrusions. The occurrence of high fO_2 conditions during magma differentiation is further supported by petrographic evidence, since oxides (especially magnetite) are common minerals in the most mafic compositions, and also by Harker diagrams for FeO_t and TiO_2 (Fig. 8), showing clear negative slopes as is typical of magma suites where the oxide minerals' fractionation has a significant role since the early stages of differentiation (e.g., Miyashiro 1974; Miyashiro and Shido 1975; McBirney 1993).

In agreement with the metaluminous and high-K calc-alkaline characteristics of the Dehsalm granitoids, almost all samples plot in the volcanic arc granites domain in the diagrams proposed by Pearce et al. (1984), with a tendency toward the syn-collision granites (Fig. 11). Low Rb/Sr ratios, with the mean value of 0.15, also fit into the described geochemical signature.

The Sr/Y and La/Yb ratios are high (31.6–72.2 and 21.5–33.5, respectively) and overlap the values reported for adakites (Kepezhinskas et al. 1997; Castillo et al. 1999). However, when the compositions are plotted in the Sr/Y–Y and La/Yb–Yb discrimination diagrams (Fig. 12a, b), Y and Yb contents are generally higher than expected in typical adakites. More importantly, two of the most typical features of adakites, as shown by Defant and Drummond (1990), are high Na_2O contents (3.5–7.5 wt%) and low K_2O/Na_2O ratio ($\sim$0.42), which clearly contrast with the K-rich compositions of the Dehsalm intrusives. The hypothesis that K enrichment could be mainly an effect of hydrothermal alteration is not supported by immobile trace element information, since the Dehsalm samples plot, in

Table 2 Rb–Sr and Sm–Nd isotopic data from seven whole-rock samples, one plagioclase separate and one biotite separate of the Dehsalm granitoids

Sample	Sr (ppm)	Rb (ppm)	$^{87}Rb/^{86}Sr$	Error (2 s)	$^{87}Sr/^{86}Sr$	Erro (2 s)	$(^{87}Sr/^{86}Sr)_i$	Nd (ppm)	Sm (ppm)	$^{147}Sm/^{144}Nd$	Error (2 s)	$^{143}Nd/^{144}Nd$	Error (2 s)	εNd_i
D6-227	1,210	49.0	0.117	0.003	0.704752	0.000024	0.704698	38.6	7.20	0.113	0.003	0.512727	0.000015	+2.08
De12	1,139	85.7	0.218	0.006	0.705179	0.000030	0.705079	34.7	6.14	0.107	0.003	0.512714	0.000012	+1.84
D4-245	1,339	80.2	0.173	0.005	0.704893	0.000027	0.704812	47.9	8.03	0.101	0.003	0.512733	0.000011	+2.25
d12-250	683.5	115.5	0.489	0.014	0.705094	0.000025	0.704867	21.6	3.62	0.101	0.003	0.512696	0.000012	+1.52
d10-67	674.8	180.3	0.773	0.022	0.705214	0.000023	0.704856	38.6	6.35	0.100	0.003	0.512710	0.000019	+1.8
De-7	1,373	63.8	0.134	0.004	0.705016	0.000038	0.704954	38.6	7.27	0.114	0.003	0.512748	0.000018	+2.49
D3-227	637	199	0.904	0.024	0.705244	0.000035	0.704825	40.1	6.73	0.102	0.003	0.512745	0.000016	+2.47
D3-227B	54	700	37.270	1.050	0.722477	0.000033	0.705224	–	–	–	–	–	–	–
D3-227P	1,204	221	0.531	0.015	0.705058	0.000035	0.704812	–	–	–	–	–	–	–

The initial ratio of $^{87}Sr/^{86}Sr$ and $^{143}Nd/^{144}Nd$ ratios were calculated an age of 33 Ma, based on the Rb–Sr date. D3-227 B and D3-227 P represent biotite and plagioclase separates, respectively, of sample D3-227

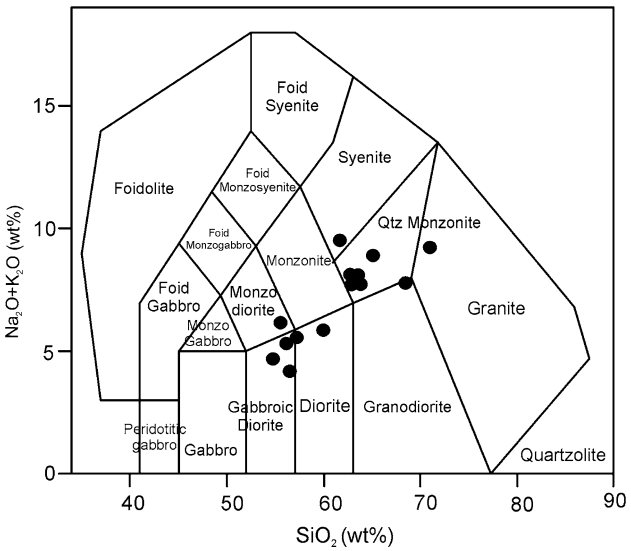

Fig. 6 Na_2O+K_2O versus SiO_2 diagram. Fields after Middlemost (1985)

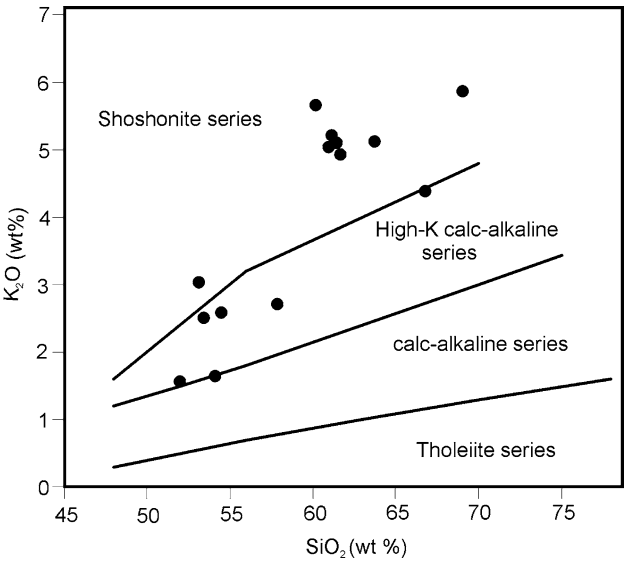

Fig. 7 K_2O versus SiO_2 diagram. Fields after Peccerillo and Taylor (1976)

the Th–Co diagram (Hastie et al. 2007), in the high-K calc-alkaline and shoshonitic series fields (Fig. 13).

Therefore, a suitable petrogenetic model for the Dehsalm granitoids must reconcile both their shoshonitic nature, as revealed by petrography and most of the geochemical data, and the "adakitic" affinity, suggested by some trace element features. A recently defined (Xiao and Clemens 2007) category of adakites (C-type) displays K-rich compositions; however, as will be discussed below, the features of the Dehsalm granitoids show that these rocks are also distinct from C-type adakites.

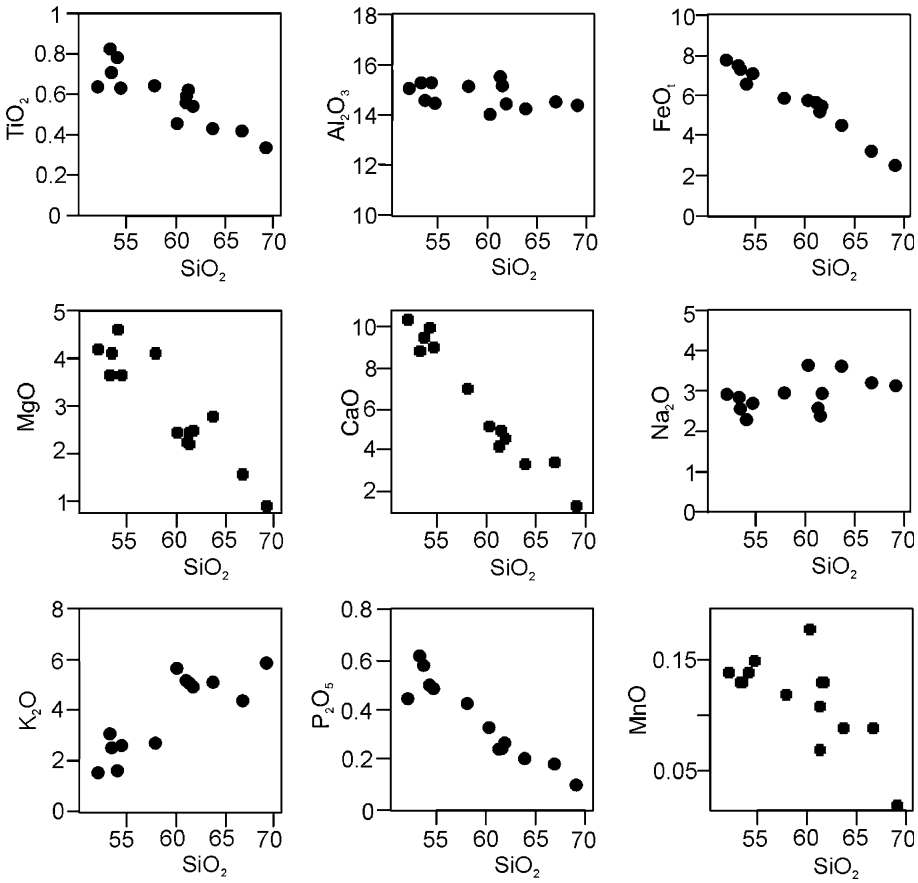

Fig. 8 Harker diagrams for the intrusive rocks of Dehsalm

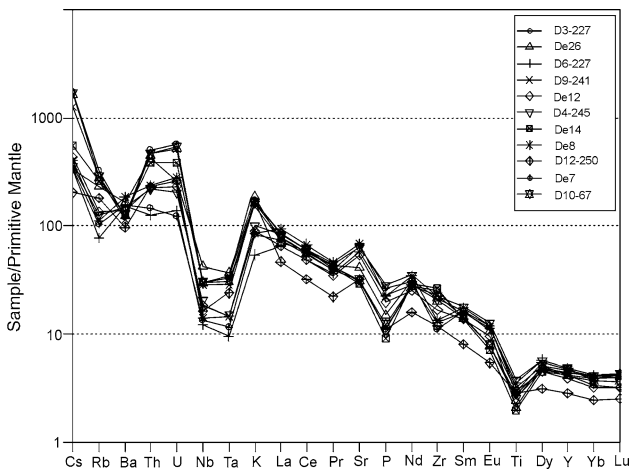

Fig. 9 Primitive mantle-normalized trace element spider diagram (Sun and McDonough 1989) for Dehsalm intrusives

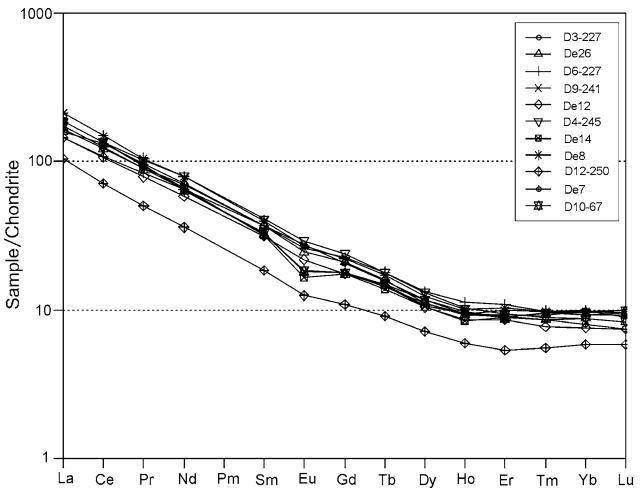

Fig. 10 Chondrite-normalized diagram (Boynton 1984), showing significant LREE enrichments and high degrees of REE fractionation for Dehsalm intrusives

Rb–Sr and Sm–Nd isotope geology

One of the least altered samples—D3-227—was selected for Rb–Sr geochronology. Biotite and plagioclase concentrates were obtained, and together with the whole-rock analysis, their Rb–Sr compositions gave an age of 33 ± 1 Ma (Fig. 14). Since the plagioclase and whole-rock data plot close to each other, the result is strongly dependent on the Sr isotopic composition of biotite and, accordingly, it must be viewed mainly as a biotite Rb–Sr age. An identical age within error (34 ± 1 Ma) was obtained (Arjmandzadeh et al. 2011) for a shallow felsic intrusive from Chah-Shaljami (~85 km to the northwest of

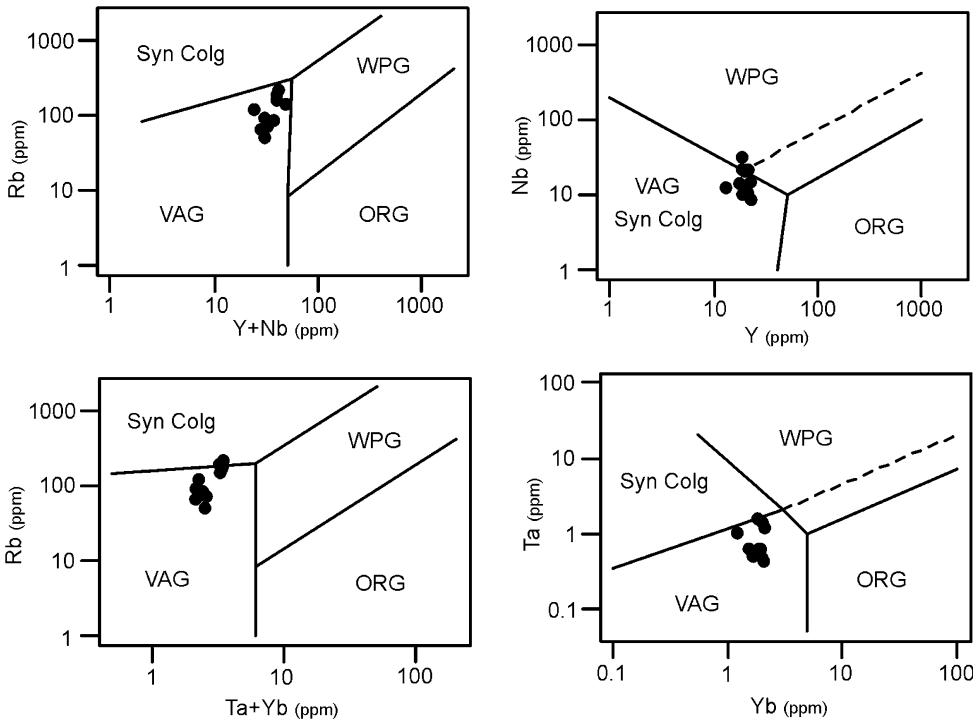

Fig. 11 Plot of the compositions of the Dehsalm intrusives on the geotectonic setting discrimination diagrams of Pearce et al. (1984) for granitoid rocks. *WPG* within-plate granites, *VAG* volcanic arc granites, *ORG* ocean ridge granites, *syn-COLG* syn-collisional granites

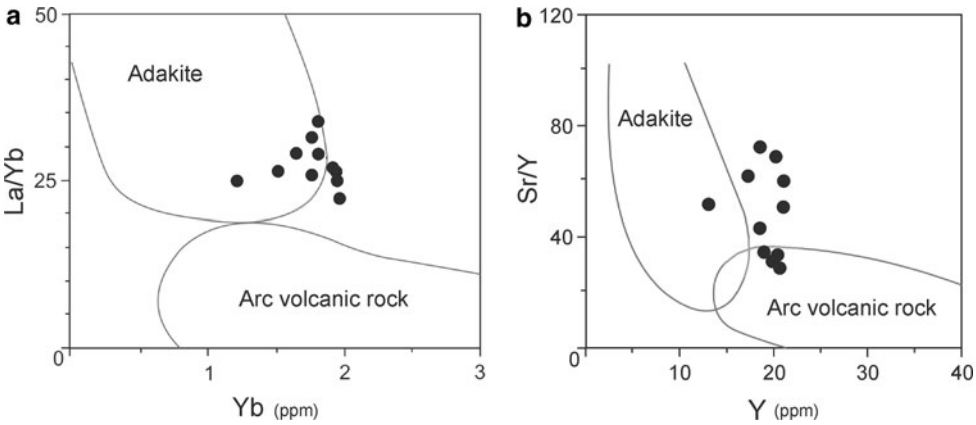

Fig. 12 **a** Plot of Dehsalm intrusives on Y versus Sr/Y diagram. Fields after Defant and Drummond (1990). **b** Plot of Dehsalm intrusives on Yb versus La/Yb diagram. Fields after Defant and Drummond (1990)

Dehsalm, again in the Lut Block; Fig. 2), which belongs to a magmatic suite displaying geochemical features similar to those shown by the granitoids studied in the present work.

Considering that the Dehsalm granitoids are subvolcanic, their post-emplacement cooling should have been fast and, therefore, the 33 Ma age may be considered as dating the magmatic event. As such, initial isotopic ratios and ε values were calculated for 33 Ma.

Sr and Nd isotopic compositions were determined for seven whole-rock samples. Initial $^{87}Sr/^{86}Sr$ and εNd values are tightly clustered in the ranges from 0.70470 to 0.70508 and from +1.5 to +2.5, respectively. In the εNd_i versus $(^{87}Sr/^{86}Sr)_i$ diagram (Fig. 15), this cluster plots to the right of the so-called mantle array and overlaps the field of island-arc basalts. These isotopic compositions also overlap almost perfectly the isotopic data obtained for Chah-Shaljami samples (Arjmandzadeh et al. 2011).

The very similar initial Sr and Nd isotopic compositions in the seven-sample cluster suggest that the Dehsalm intrusions are co-genetic, deriving from the same parental magmas by magmatic differentiation processes. Taking into account the IAB-like isotopic compositions of the studied rocks, the parental magmas may have been formed by partial melting in a supra-subduction mantle wedge (Stolz et al. 1996). The occurrence of gabbroic rocks in the Dehsalm suite provides additional evidence in favor of an origin of the parental magmas by melting of mantle peridotites, rather than by melting of mafic crust.

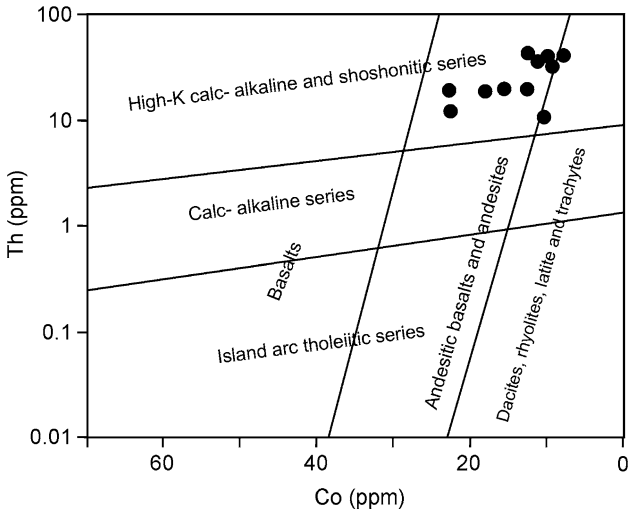

Fig. 13 Plot of Deshalm intrusives in the Th–Co diagram. Fields after Hastie et al. (2007). *Subhorizontal boundaries* separate fields of magma series typical of subduction-related settings. *Subvertical boundaries* separate fields of volcanic rocks in those settings

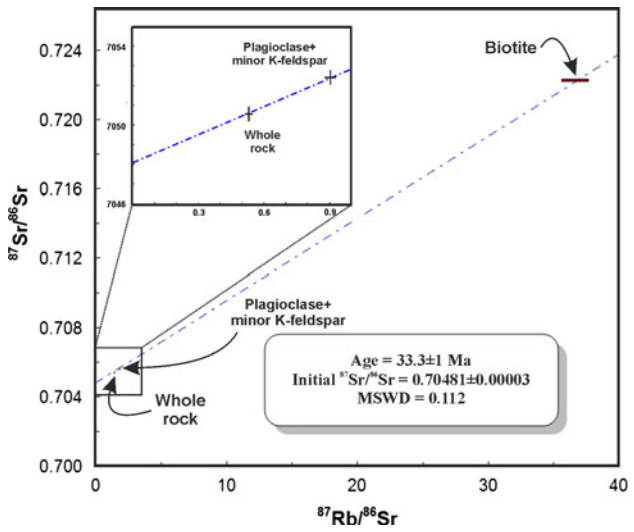

Fig. 14 Plot of the whole rock–plagioclase–biotite isochron of sample D3-227

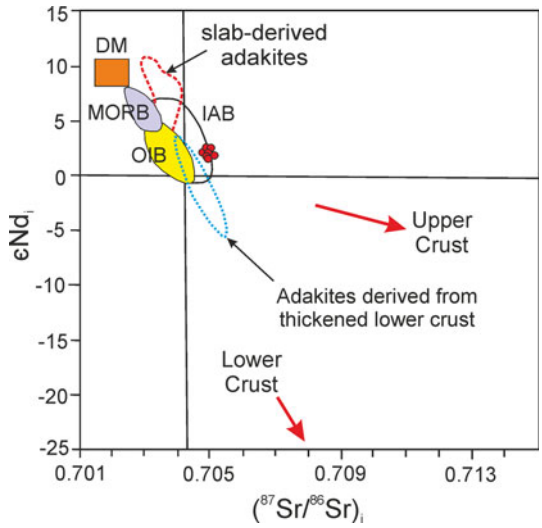

Fig. 15 εNd_i-$(^{87}Sr/^{86}Sr)_i$ diagram for the Dehsalm intrusive rocks. The field of Cenozoic subducted oceanic crust-derived adakites was defined after Defant et al. (1992), Kay et al. (1993), Sajona et al. (2000) and Aguillón-Robles et al. (2001). The data for adakitic rocks directly derived from a thick lower crust are after Atherton and Petford (1993), Muir et al. (1995) and Petford and Atherton (1996). *MORB* mid-ocean ridge basalts, *DM* depleted mantle, *OIB* ocean-island basalts, *IAB* island-arc basalts. Initial ratios calculated for 33 Ma

Discussion

Origin of the parental magmas

Some relevant geochemical features of Dehsalm intrusives—such as the high Sr/Y and La/Yb ratios, and the low HREE contents—are similar to those exhibited by adakites. These characteristics could be a consequence of melting of garnet amphibolite or eclogite facies rocks that may be found in subducted oceanic crust (Defant and Drummond 1990). However, other sources of adakitic parental magmas have been proposed, such as hydrous mantle peridotite (Stern and Hanson 1991), mafic rocks at the base of thickened lower crust (Zhang et al. 2001; Chung et al. 2003; Xiong et al. 2003; Hou et al. 2004; Wang et al. 2005; Guo et al. 2006) or delaminated mafic lower crust (e.g., Kay and Kay 1993; Defant et al. 2002; Gao et al. 2004; Guo et al. 2006; Lai et al. 2007; Liu et al. 2008a, b). Some authors (e.g., Castillo et al. 1999; Macpherson et al. 2006) consider that assimilation-fractional crystallization (AFC) processes must be taken into account to explain the genesis of the adakitic rocks.

The high Sr/Y and La/Yb ratios could be attributed to the retention of Y and HREE in residual garnet and hornblende (Defant and Drummond 1990). The strong LREE/HREE fractionation in adakites is classically interpreted as reflecting the presence of garnet and amphibole in the residue resulting from the partial melting of their source, whereas those minerals are not residual phases during the genesis of typical of the most common calc-alkaline magmas (Martin 1986). In this case, although not truly adakitic, the Dehsalm suite could be related to a garnet- and/or amphibole-bearing magma source.

The Ti–Nb–Ta negative anomalies are typical of all types of calc-alkaline magmas, and they may be explained by residual hornblende and/or Fe–Ti oxides (rutile, ilmenite) in the source of the parental magmas (Pearce and Norry 1979). However, since Nb and Ta are both highly incompatible in typical mantle assemblages and immobile during metasomatic events, their anomalies can, alternatively, be explained by the addition of slab components to

the mantle wedge causing increase in several incompatible elements (namely LILE), but not in Nb and Ta (e.g., Turner et al. 2003; Wang et al. 2006; Tamura et al. 2011).

The plot of the Dehsalm samples on the εNd_i—$(^{87}Sr/^{86}Sr)_i$ diagram (Fig. 15) shows that their compositions do not fit into an origin of the parental magmas by melting of thick lower crust or Cenozoic subducted oceanic crust as proposed for typical adakites. In contrast, they have Sr and Nd isotopic composition very similar to those of normal island-arc basalts, pointing to melting in a mantle wedge followed by magmatic differentiation.

Experimental studies demonstrate that Mg# is a useful index to discriminate melts purely derived from the crust from those coming from the mantle. Adakitic magmas, whether derived directly from partial melting of the subducted oceanic slab (MORB) or from lower crustal mafic rocks, usually show low Mg# (<40), regardless of melting degrees (Rapp and Watson 1995), while the studied intrusives have moderately high Mg#, varying from 40.1 to 55.6, thus providing additional evidence for the involvement of a mantle source in the origin of the parental melts. The occurrence, at Dehsalm, of mafic lithologies, with gabbro-dioritic compositions, also supports the hypothesis of a peridotitic mantle source.

The studied rocks, although displaying some resemblances with adakites, are markedly enriched in some elements, such as K and Rb, revealing a high-K calc-alkaline to shoshonitic signature.

The high potassium contents can be explained by decomposition of a K-rich phase (probably phlogopite) during the partial melting of a previously metasomatized mantle peridotite (Conceição and Green 2004).

Ascent of magmas through thickened continental crust could have been the cause of crustal contamination resulting in higher Rb/Sr and LILE/HFSE ratios and increase in K_2O and Th contents due to assimilation and fractional crystallization (AFC) processes (Esperanca et al. 1992). However, if such mechanisms had extensively occurred, significant variation in Sr–Nd isotopic composition would become evident and correlations of isotopic ratios with SiO_2 should be expected (Castillo et al. 1999). In addition, the very restricted range of both $(^{87}Sr/^{86}Sr)_i$ and εNd_i precludes assimilation and fractional crystallization (AFC) as a major process in the generation of the diverse magma compositions of the Dehsalm suite. As such, high Rb/Sr and K_2O values are most likely attributed to the source geochemistry. Ionov and Hofmann (1995) have shown from mantle xenoliths that amphiboles can have high K and very low Rb concentration while coexisting phlogopite is rich in both K and Rb. Thus, a strong participation of phlogopite decomposition (but not necessarily its complete melting) in the generation of the parental magmas would account for the potassium-rich nature and high Rb/Sr ratios displayed by the Dehsalm intrusives. Metasomatism of mantle peridotite by slab melts produces orthopyroxene, clinopyroxene, garnet, phlogopite, and richterite or pargasite (Sen and Dunn 1994; Rapp et al. 1999; Prouteau et al. 2001).

Hypotheses on the processes in the mantle source suffer from the fact that, as is common in studies on subduction-related magmatism (e.g., Turner et al. 2003, 2011), none of the Dehsalm samples (Mg# $\leq$ 55.6) represents directly a primary magma and, consequently, magma differentiation has also played a role even in the most mafic compositions. However, taking the complete set of geochemical evidence into account, probably the parental magmas originated by partial melting of metasomatized mantle peridotite. Contribution of phlogopite breakdown to the primitive melts would cause the high potassium contents, responsible for the shoshonitic signature of the studied rocks. Additionally, residual garnet and amphibole may have enhanced the LREE/HREE fractionation. The amphibole contribution could have taken place also as low-P fractionation, and therefore, its presence in the mantle source is not required. The role of garnet as a residual mantle phase is also debatable, taking into account that the high LREE/HREE ratios are accompanied by only small HREE fractionation (Fig. 10). In fact, Lin et al. (1989) have shown that, in some cases, melting processes in spinel peridotite sources may produce magmas with LREE enrichment but flat HREE. Turner et al. (2003) used the Tb/Yb ratio as an indicator of the participation of garnet in residual assemblages, and according to their modelling for the genesis of parental magmas of K-rich suites in a volcanic arc setting, Tb/Yb values around 0.4 (such as those obtained in the Dehsalm rocks) fit into a scenario of small amounts ($\sim$3 %) of residual garnet.

C-type adakites (Xiao and Clemens 2007), which have some geochemical resemblance to the studied rocks, have been interpreted as post-collisional granitoids resulting from melting of K-rich (meta-)basaltic, dioritic or tonalitic rocks at the base of overthickened crust and under a very strong geothermal gradient. Examples studied by Xiao and Clemens (2007) correspond to silicic magmas, with low Mg# and an isotope signature suggesting a source with a long crustal residence period ($\varepsilon Nd_i = -18.7$; $^{87}Sr/^{86}Sr_i = 0.708048$). In contrast, Dehsalm rocks include lithologies more mafic than typical C-type adakites and have relatively high Mg#, positive εNd_i values and low $^{87}Sr/^{86}Sr_i$ ratios. Moreover, several lines of evidence suggest that during the Oligocene, the Lut Block was at the Neothethysian margin of the central Iran microcontinent (Shafiei et al. 2009) and not in a post-collisional setting.

Tectonomagmatic and metallogenic implications

Arjmandzadeh et al. (2011) recently proposed a two-sided asymmetric subduction model to explain the tectonomagmatic setting of the Lut Block. This model relates the voluminous Tertiary magmatism within the Lut Block to fast west-directed subduction and the abundant structural evidence in the Afghan Block to slower eastward subduction, in agreement with the correlation between convergence rate and volume of magmatism along subduction zones that Tatsumi and Eggins (1995) have shown to exist. The larger volumes of subduction predicted along west-directed slabs should favor the formation of greater amounts of arc-related magmas, as reported within the Lut Block.

A period of important magmatism and mineralization took place from middle Eocene to early Oligocene in the Lut Block. The location of major Tertiary mineralization occurrences within the Lut Block is shown in Fig. 16. Tarkian et al. (1983) ascribed an island-arc signature to late Eocene (42 Ma) to mid-Oligocene (31.4 Ma) volcanic rocks of Khur and Shurab from the Ferdows and Mud areas. K-rich calc-alkaline to shoshonitic andesitic rocks from Qaleh-Zari Cu–Au–Ag IOCG were dated at 40.5 ± 2 Ma by Kluyver et al. (1978). The Hired intrusion-hosted Au deposit is reported by Eshraghi et al. (2010) to be related to a post-Eocene quartz diorite porphyry stock intruded into Eocene andesitic volcanic, pyroclastic and sedimentary rocks. Malekzadeh (2009) inferred an island-arc tectonomagmatic setting for the middle Eocene (39 Ma) intermediate subvolcanic rocks of the Maherabad and Khopik Cu–Au porphyry deposit.

Chah-Shaljami porphyritic granitoids were dated by Arjmandzadeh et al. (2011), using the Rb–Sr isotopic systematics of minerals and whole rock, at 33.5 ± 1 Ma. Richards et al. (2012) obtained an identical age (33.72 ± 0.08 Ma), within error, using the $^{40}Ar/^{39}Ar$ method in a sample from a quartz monzonite intrusion from the same area. The Chah-Shaljami rocks constitute a suite with high-K calc-alkaline features, although some trace element characteristics reveal an adakitic affinity. These granitoids plot almost completely in the field of the volcanic arc granites; however, they also straddle the boundary to the syn-collision granites. $(^{87}Sr/^{86}Sr)_i$ and εNd_i isotopic ratios of Chah-Shaljami intrusives range from 0.70470 to 0.70506 and from +1.9 to +2.7, respectively, which fits into a supra-subduction mantle wedge source for the parental melts. The gathered data on alteration, mineralization and hydrothermal fluids together with field evidence indicate a deep Cu-Mo porphyry system in the Chah-Shaljami area.

The data presented in this work reveal that the Dehsalm subvolcanics are not only contemporaneous (33 ± 1 Ma) but also have very similar geochemical and isotope signatures compared to Chah-Shaljami granitoids, revealing that the intrusions of the two areas are testimonies of the

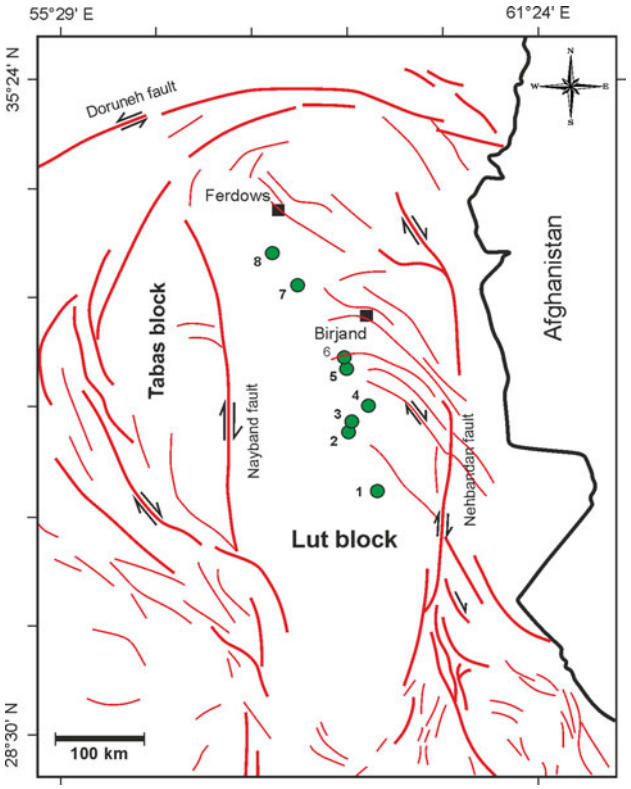

Fig. 16 Major Tertiary mineralization occurrences associated with the Eocene–Miocene magmatism within the Lut Block. *1* Dehsalm Cu–Mo porphyry (Arjmandzadeh et al. 2013); *2* Chah-Shaljami Cu–Mo porphyry (Arjmandzadeh et al. 2011); *3* Qlaleh zari Cu–Au–Ag IOCG (Kluyver et al. 1978); *4* Hired Au–Sn associated with reduced granitoids (Eshraghi et al. 2010); *5* Khopik Cu–Au porphyry (Malekzadeh 2009); *6* Maherabad Cu–Au porphyry (Malekzadeh 2009); *7* Khur Cu–Pb–Zn–Sb vein-type mineralization (Tarkian et al. 1983); *8* Shurab Cu–Pb–Zn–Sb vein-type mineralization (Tarkian et al. 1983)

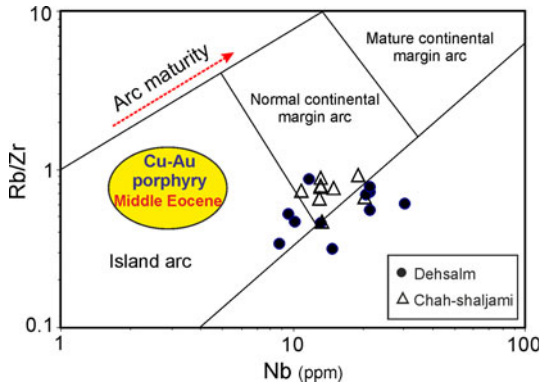

Fig. 17 Plot of Rb/Zr–Nb for Dehsalm intrusive rocks. Fields after Brown et al. (1984). The field of Cu–Au porphyry was drawn mainly on the basis of Maher-abad and Khoopic prospects (after Malekzadeh 2009). The data for Chah-Shaljami are after Arjmandzadeh et al. (2011)

same type of magmatic processes. Additionally, studies on the ore-forming processes in Dehsalm (Arjmandzadeh et al. 2013) concluded that a Cu–Mo porphyry-type mineralization system also existed in this area.

A spatial and temporal relationship between tectono-magmatic cycles in arc mineralization processes has long been recognized, with porphyry Cu deposits typically occurring in subduction-related settings, especially in continental arcs (e.g., Sillitoe 1988; Sillitoe and Bonham 1984), in relation to oxidized I-type granitoids. The relative importance of Cu and Mo in those deposits seems to be controlled by the water content of the initial magma, the water saturation level in each situation and the degree of crystal fractionation required to achieve water saturation (Candela and Holland 1984, 1986; Strong 1988; Candela 1992). Cu–Au porphyry deposits are usually considered more typical of relatively immature arcs (Cooke et al. 1998; Laznicka 2010), although they are also found in the Andean arc, as in the Maricunga belt, Chile (Vila and Sillitoe 1991).

The plot of geochemical data obtained for igneous rocks of the Lut Block on the Rb/Zr–Nb diagram (Brown et al. 1984; Fig. 17) agrees with that general picture. In fact, rocks with associated Cu-Au deposits have mid-Eocene age and lie in the island-arc field, while the Oligocene granitoids with Mo-bearing deposits (this work and Arjmandzadeh et al. 2011) display features of a more mature arc setting (Fig. 17), probably in relation to crustal thickening accompanying the beginning of the collision of the Afghan and Lut plates.

Sillitoe (1998) remarked that crustal thickening associated with compressive tectonism was synchronous with the formation of giant porphyry copper systems in central and northern Chile, southwest Arizona, Irian Jaya and Iran. The existence of a thick crust (40–48 km) in the Lut Block was suggested by Dehghani and Makris (1983). More recently, Hatzfeld and Molnar (2010) after comparing structural evidence from the Himalaya and the adjacent Tibetan Plateau, on the one hand, and from Zagros and the Iranian Plateau, on the other hand, concluded that crustal thickening occurred beneath short ranges that link strike-slip faults in the region surrounding the Lut Block. Therefore, the geodynamic setting of the Oligocene subvolcanic intrusives of the Lut Block seems to fit into the conditions favorable to the genesis of important porphyry copper deposits.

Conclusions

A Rb–Sr biotite date yields an intrusion age of 33 ± 1 Ma for the Dehsalm granitoids in the Lut Block volcanic–plutonic belt. These granitoids display trace element features typical of the magmatism related to a subduction zone, such as LILE enrichment and marked Nb, Ta and Ti negative anomalies. Geochemical evidence shows that the Dehsalm intrusives are high-K calc-alkaline to shoshonitic. They also belong to the magnetite series, with mineral potential for Cu–Mo (–Au–Pb–Zn), as detected by geochemical exploration surveys (Arjmandzadeh et al. 2013). Some geochemical resemblance, namely the high LREE/HREE ratios, between Dehsalm granitoids and adakitic rocks can be attributed to the presence of residual garnet and amphibole in a mantle source. The relatively high Mg# values discard a crustal origin (subducted slab or lower crust) for the parental magmas. Isotope geochemistry shows that the studied rocks are co-genetic and should be related to each other mainly by magmatic differentiation processes, such as fractional crystallization. Therefore, the high K_2O contents should result from the mantle source geochemistry, rather than from important assimilation of crustal materials. Despite the fact that no primitive melt is directly represented by any of the studied rocks, some hypotheses on the processes involving the mantle source may be put forward: The parental magmas probably derived from partial melting of metasomatized peridotite in a supra-subduction mantle wedge; during the melting event, phlogopite breakdown should have contributed to some of the most important geochemical fingerprints of the suite; garnet and amphibole possibly remained as residual phases in the source. This study provides new evidence for subduction beneath the Lut Block during the Tertiary. A spatial and temporal relationship between tectono-magmatic cycles in the eastern Iran arc and porphyry Cu–(Mo–Au) formation has been recognized. Cu–Au porphyry deposits of the Lut Block seem to be related to an immature arc geotectonic setting during the middle Eocene, while Mo-bearing porphyry-type deposits correspond to a more advanced stage of arc evolution and probably to crustal thickening as a result of the beginning of Afghan and Lut plate collision during Oligocene.

Acknowledgments The authors wish to thank Mrs. Sara Ribeiro (Laboratório de Geologia Isotópica da Universidade de Aveiro) for the TIMS analysis and for the guidance and assistance during sample preparation in the clean room. Dr. Jorge Medina is acknowledged for the help in planning and scheduling the stay of Reza Arjmandzadeh in Aveiro. This research was financially supported by the Geobiotec Research Unit (funded by the Portuguese Foundation for Science and Technology, through project PEst-C/CTE/UI4035/2011), University of Aveiro, Portugal. Ministry of Sciences, Research and Technology of Iran is thanked for financial support for sabbatical research of Reza Arjmandzadeh in Portugal. National Iranian Copper Industries Company is thanked for the assistance with drill hole studies. A group of engineers from the NE branch of Geological Survey of Iran—especially Azmi, Jafari and Askari—are acknowledged for cooperation in the fieldwork. The authors also would like to thank the two reviewers, Charles R. Stern and Saeed Alirezaei, as well as Marlina Elburg (subject editor) and Wolf-Christian Dullo (editor in chief), for

the constructive comments that greatly contributed to the improvement of the manuscript.

References

Aguillón-Robles A, Caimus T, Bellon H, Maury RC, Cotton J, Bourgois J, Michaud F (2001) Late Miocene adakites and Nb-enriched basalts from Vizcaino Peninsula, Mexico: indicators of East Pacific Rise subduction below southern Baja California. Geology 29:531–534

Arjmandzadeh R, Karimpour MH, Mazaheri SA, Santos JF, Medina J, Homam SM (2011) Sr–Nd isotope geochemistry and petrogenesis of the Chah-Shaljami granitoids (Lut Block, Eastern Iran). J Asian Earth Sci 41:283–296

Arjmandzadeh R, Karimpour MH, Mazaheri SA, Santos JF, Medina J, Homam SM (2013) Petrogenesis, tectonomagmatic setting and mineralization potential of Dehsalm granitoids, Lut block, Eastern Iran. Geosci Sci Q J 22:3–13

Atherton MP, Petford N (1993) Generation of sodium-rich magmas from newly underplated basaltic crust. Nature 362:144–146

Bagheri B, Stampfli GM (2008) The Anarak, Jandaq and Posht-e-Badam metamorphic complexes in central Iran: new geological data, relationships and tectonic implications. Tectonophysics 451:123–155. doi:10.1016/j.tecto.2007.11.047

Berberian M (1983) Continental deformation on the Iranian Plateau. Geol Surv Iran, report no. 52

Berberian M, King GC (1981) Towards a paleogeography and tectonic evolution of Iran. Can J Earth Sci 18:210–265

Berberian M, Jackson JA, Qorashi M, Khatib MM, Priestley K, Talebian M, Ghafuri-Ashtiani M (1999) The 1997 may 10 Zirkuh (Qaenat) earthquake (Mw 7.2): faulting along the Sistan suture zone of eastern Iran. Geophys J Int 136:671–694

Boynton WV (1984) Geochemistry of the rare earth elements: meteorite studies. In: Henderson P (ed) Rare earth element geochemistry. Elsevier, Amsterdam, pp 63–114

Brown GC, Thorpe RS, Webb PC (1984) The geochemical characteristics of granitoids in contrasting arcs and comments on magma sources. J Geol Soc London 141:413–426

Camp VE, Griffis RJ (1982) Character, genesis and tectonic setting of igneous rocks in the Sistan suture zone, eastern Iran. Lithos 15:221–239

Candela PA (1992) Controls on ore metal ratios in granite related ore systems: an experimental and computational approach. Trans R Soc Edinb Earth Sci 83:317–326

Candela PA, Holland HD (1984) The partitioning of copper and molybdenum between silicate melts and aqueous fluids. Geochim Cosmochim Act 48:373–380

Candela PA, Holland HD (1986) A mass transfer model for copper and molybdenum in magmatic hydrothermal systems: the origin of porphyry-type copper deposits. Econ Geol 81:1–18

Castillo PR, Janney PE, Solidum RU (1999) Petrology and geochemistry of Camiguin Island, southern Philippines: insights to the source of adakites and other lavas in a complex arc setting. Contrib Miner Petrol 134:33–51

Chappell BW, White AJR (1992) I- and S-type granites in the Lachlan fold belt. Trans R Soc Edinb Earth Sci 83:1–26

Chung S-L, Liu D, Ji J, Chu M-F, Lee H-Y, Wen D-J, Lo C-H, Lee T-Y, Qian Q, Zhang Q (2003) Adakites from continental collision zones: melting of thickened lower crust beneath southern Tibet. Geology 31:1021–1024

Conceição RV, Green DH (2004) Derivation of potassic (shoshonitic) magmas by decompression melting of phlogopite + pargasite lherzolite. Lithos 72:209–229

Cooke DR, Heithersay PS, Wolfe RC, Calderon AL (1998) Australian and western Pacific porphyry Cu–Au deposits. J Aust Geol Geophys 17:97–104

Defant MJ, Drummond MS (1990) Derivation of some modern arc magmas by melting of young subducted lithosphere. Nature 347:662–665

Defant MJ, Jackson TE, Drummond MS, De Boer JZ, Bellon H, Feigenson MD, Maury RC, Stewart RH (1992) The geochemistry of young volcanism throughout western Panama and southeastern Costa Rica: an overview. J Geol Soc London 149:569–579

Defant MJ, Xu J-F, Kepezhinskas P, Wang Q, Zhang Q, Xiao L (2002) Adakites: some variations on a theme. Acta Petrol Sin 18:129–142

Dehghani A, Makris J (1983) The gravity field and crustal structure of Iran, Geodynamic project (Geotraverse) in Iran. Geol surv Iran, Report no. 51

Dercourt J, Gaetani M, Vrielynck B, Barrier E, Biju-Duval B, Brunet M-F, Cadet JP, Crasquin S, Sandulescu M (eds) (2000) Atlas Peri-Tethys Paleogeographical Maps, vol I–XX. CCGM/CGMW, Paris, pp 1–269. 24 maps and explanatory note

Dilles JH (1987) Petrology of the Yerington Batholith, Nevada: evidence for evolution of porphyry copper ore fluids. Econ Geol 82:1750–1789

Drake MJ, Weill DF (1975) Partition of Sr, Ba, Ca, Y, Eu^{2+}, Eu^{3+} and other REE between plagioclase feldspar and magmatic liquid: an experimental study. Geochim Cosmochim Act 39:689–712

Eastoe CG, Eadington PJ (1986) High-temperature fluid inclusions and the role of the biotite granodiorite in mineralization at the Panguna porphyry copper deposit, Bougainville, Papua New Guinea. Econ Geol 81:478–483

Eftekharnejad J (1981) Tectonic division of Iran with respect to sedimentary basins. J Iran Petroleum Soc 82:19–28

Eshraghi H, Rastad E, Motevali K (2010) Auriferous sulfides from Hired gold mineralization, South Birjand, Lut block, Iran. J Miner Petrol Sci 105:167–174

Esmaeily D (2005) Petrology of the Jurassic Shah-Kuh granite (eastern Iran), with reference to tin mineralization. J Asian Earth Sci 25:961–980

Esperanca S, Crisci M, de Rosa R, Mazzuli R (1992) The role of the crust in the magmatic evolution of the island Lipari (Aeolian Islands, Italy). Contrib Miner Petrol 112:450–462

Gao S, Rudnick R, Yuan HL, Liu XM, Liu YS, Xu WL, Ling WL, Ayers J, Wang XC, Wang QH (2004) Recycling lower continental crust in the north China craton. Nature 432:892–897

Gill JB (1981) Orogenic andesites and plate tectonics. Springer, New York

Golonka J (2004) Plate tectonic evolution of the southern margin of Eurasia in the Mesozoic and Cenozoic. Tectonophysics 38:235–273. doi:10.1016/j.tecto.2002.06.004

Griffis R, Meixner H, Johns G, Abedian N (1992) Geological quadrangle map of Iran No. K9. Geol Surv Iran

Guo F, Fan WM, Li CW (2006) Geochemistry of late Mesozoic adakites from the Sulu belt, eastern China: magma genesis and implications for crustal recycling beneath continental collisional orogens. Geol Mag 143:1–13

Gust DA, Arculus RJ, Kersting AB (1997) Aspects of magma sources and processes in the Honshu arc. Can Mineral 35:347–365

Hastie AR, Kerr AC, Pearce JA, Mitchell SF (2007) Classification of altered volcanic island arc rocks using immobile trace elements:

development of the Th–Co discrimination diagram. J Petrol 48:2341–2357
Hatzfeld D, Molnar P (2010) Comparisons of the kinematics and deep structures of the Zagros and Himalaya and of the Iranian and Tibetan plateaus and geodynamic implications. Rev Geophys 48:RG2005. doi:10.1029/2009RG000304
Henderson P (1984) Rare earth element geochemistry. Elsevier, Amsterdam
Hou Z-Q, Gao Y-F, Qu X-M, Rui Z-Y, Mo X–X (2004) Origin of adakitic intrusives generated during mid-Miocene east-west extension in southern Tibet. Earth Planet Sci Lett 220: 139–155
Ionov DA, Hofmann AW (1995) Na–Ta-rich mantle amphiboles and micas: implications for subduction-related metasomatic trace element fractionations. Earth Planet Sci Lett 131:341–356
Kay RW, Kay SM (1993) Delamination and delamination magmatism. Tectonophysics 219:177–189
Kay SM, Ramos VA, Marquez M (1993) Evidence in Cerro Pampa volcanic rocks of slab melting prior to ridge trench collision in southern South America. J Geol 101:703–714
Kepezhinskas PK, McDermott F, Defant MJ, Hochstaedter FG, Drummond MS, Hawkesworth CJ, Koloskov A, Maury RC, Bellon H (1997) Trace element and Sr–Nd–Pb isotopic constraints on a three-component model of Kamchatka arc petrogenesis. Geochim Cosmochim Act 61:577–600
Kluyver HM, Griffts RJ, Tirrul R, Chance PN, Meixner HM (1978) Explanatory text of the Lakar Kuh quadrangle 1:250,000. Geol Surv Iran 19:1–175
Lai SC, Qin JF, Li YF (2007) Partial melting of thickened Tibetan Crust: geochemical evidence from Cenozoic adakitic volcanic rocks. Int Geol Rev 49:357–373
Laznicka P (2010) Giant metallic deposits: future sources of industrial metals. Springer, Berlin-Heidelberg
Lin PN, Stern RJ, Bloomer SH (1989) Shoshonitic volcanism in the northern Mariana arc: 2. Large ion lithophile and rare earth element abundances: evidence for the source of incompatible element enrichments in intraoceanic arcs. J Geophys Res 94:497–514
Liu S, Hu RZ, Feng CX, Zou HB, Li C, Chi XG, Peng JT, Zhong H, Qi L, Qi YQ, Wang T (2008a) Cenozoic high Sr/Y volcanic rocks in the Qiangtang terrane, northern Tibet: geochemical and isotopic evidence for the origin of delaminated lower continental melts. Geol Mag 145:463–474
Liu S, Hu RZ, Gao S, Feng CX, Qi YQ, Wang T, Feng GY, Coulson IM (2008b) U–Pb zircon age, geochemical and Sr–Nd–Pb–Hf isotopic constraints on age and origin of alkaline intrusions and associated mafic dikes from Sulu orogenic belt, Eastern China. Lithos 106:365–379
Macpherson CG, Dreher ST, Thirlwall MF (2006) Adakites without slab melting: high pressure differentiation of island arc magma, Mindanao, the Philippines. Earth Planet Sci Lett 243:581–593
Malekzadeh A (2009) Geology, mineralization, alteration, geochemistry, microthermometry, isotope studies and determining the mineralization source of Khoopic and Maherabad exploration areas. Ph.D thesis. Ferdowsi University of Mashhad
Martin H (1986) Effect of steeper Archaean geothermal gradient on geochemistry of subduction-zone magmas. Geology 14:753–756
Martin H (1999) The adakitic magmas: modern analogues of Archaean granitoids. Lithos 46:411–429
Mason DR, McDonald JA (1978) Intrusive rocks and porphyry copper occurrences of the Papua New Guinea–Solomon Islands region. Econ Geol 73:857–877
McBirney AR (1993) Igneous petrology. Jones and Bartlett Publishers, Boston
Middlemost EAK (1985) Naming materials in the magma/igneous rock system. Earth-Sci Rev 37:215–224
Miyashiro A (1974) Volcanic rock series in island arcs and active continental margins. Am J Sci 274:321–355
Miyashiro A, Shido F (1975) Tholeiitic and calc-alkalic series in relation to the behaviours of titanium, vanadium, chromium and nickel. Am J Sci 275:265–277
Muir RJ, Weaver SD, Bradshaw JD, Eby GN, Evans JA (1995) Geochemistry of the Cretaceous Separation Point batholith, New Zealand: granitoid magmas formed by melting of mafic lithosphere. J Geol Soc London 152:689–701
Pearce JA (1983) Role of the sub-continental lithosphere in magma genesis at active continental margins. In: Hawkesworth CJ, Norry MJ (eds) Continental basalts and mantle xenoliths. Shiva, Nantwich, pp 230–249
Pearce JA, Norry MJ (1979) Petrogenetic implications of Ti, Zr, Y, and Nb variations in volcanic rocks. Contrib Miner Petrol 69:33–47
Pearce JA, Harris NBW, Tindle AG (1984) Trace element discrimination diagrams for the tectonic interpretation of granitic rocks. J Petrol 25:956–983
Peccerillo A, Taylor SR (1976) Geochemistry of Eocene calc-alkaline volcanic rocks from the Kastamonu area, northern Turkey. Contrib Miner Petrol 58:63–81
Petford N, Atherton M (1996) Na-rich partial melts from newly underplated basaltic crust: the Cordillera Blanca Batholith, Peru. J Petrol 37:1491–1521
Prouteau G, Scaillet B, Pichavant M, Maury R (2001) Evidence for mantle metasomatism by hydrous silicic melts derived from subducted oceanic crust. Nature 410:197–200
Rapp RP, Watson EB (1995) Dehydration melting of metabasalt at 8–32 kbar: implications for continental growth and crust-mantle recycling. J Petrol 36:891–931
Rapp RP, Shimizu N, Norman MD (1999) Reaction between slab-derived melts and peridotite in the mantle wedge: experimental constraints at 3.8 GPa. Chem Geol 160:335–356
Richards JP, Spell T, Rameh E, Razique A, Fletcher T (2012) High Sr/Y magmas reflect arc maturity, high magmatic water content, and porphyry Cu ± Mo ± Au potential: examples from the Tethyan arcs of Central and Eastern Iran and Western Pakistan. Econ Geol 107:295–332
Sajona FG, Maury RC, Prouteau G, Cotten J, Schiano P, Bellon H, Fontaine L (2000) Slab melt as metasomatic agent in island arc magma mantle sources, Negros and Batan (Philippines). Isl Arc 9:472–486
Sen C, Dunn T (1994) Dehydration melting of a basaltic composition amphibolite at 1.5 and 2.0 GPa: implications for the origin of adakites. Contrib Miner Petrol 117:394–409
Sengör AMC, Natalin BA (1996) Paleotectonics of Asia: fragment of a synthesis. In: An Y, Harrison TM (eds) The tectonic evolution of Asia. Cambridge University Press, Cambridge, pp 486–640
Shafiei B, Haschke M, Shahabpour J (2009) Recycling of orogenic arc crust triggers porphyry Cu mineralization in Kerman Cenozoic arc rocks, southeastern Iran. Miner Deposita 44:265–283
Sillitoe RH (1988) Epochs of intrusion-related copper mineralization in the Andes. J S Am Earth Sci 1:89–108
Sillitoe RH (1998) Major regional factors favouring large size, high hypogene grade, elevated gold content and supergene oxidation and enrichment of porphyry copper deposits. In: Porter TM (ed) Porphyry and hydrothermal copper and gold deposits: a global perspective. Australian Mineral Foundation, Adelaide, pp 21–34
Sillitoe RH, Bonham HF Jr (1984) Volcanic landforms and ore deposits. Econ Geol 79:1286–1298
Stern RA, Hanson GN (1991) Archean high-Mg granodiorite: a derivative of light rare earth element enriched monzodiorite of mantle origin. J Petrol 32:201–238
Stöcklin J (1972) Lexique Stratigraphique International, vol. III, Fascicule 9b, Iran

Stolz AJ, Jochum KP, Spettel B, Hofman AW (1996) Fluid and melt-related enrichment in the subarc mantle: evidence from Nb/Ta variations in island-arc basalts. Geology 24:587–590

Strong DF (1988) A review and model for granite-related mineral deposits. CIM AN CONF 39:424–445

Sun SS, McDonough WF (1989) Chemical and isotopic systematics of oceanic basalts: implications for mantle composition and processes. Geol Soc SP 42:313–345

Tamura Y, Ishizuka O, Stern RJ, Shukuno H, Kawabata H, Embley RW, Hirahara Y, Chang Q, Kimura J-I, Tatsumi Y, Nunokawa A, Bloomer SH (2011) Two primary basalt magma types from Northwest Rota-1 Volcano, Mariana arc and its mantle diapir or mantle wedge plume. J Petrol 52:1143–1183

Tarkian M, Lotfi M, Baumann A (1983) Tectonic, magmatism and the formation of mineral deposits in the central Lut, east Iran. Ministry of Mines and Metals, Geol Surv Iran, Geodynamic Project (Geotraverse) in Iran, No. 51, pp 357–383

Tatsumi Y, Eggins S (1995) Subduction zone magmatism. Blackwell Science, Cambridge

Tirrul R, Bell IR, Griffis RJ, Camp VE (1983) The Sistan suture zone of eastern Iran. Geol Soc Am Bull 94:134–150

Turner S, Foden J, George R, Evans P, Varne R, Elburg M, Jenner G (2003) Rates and processes of potassic magma evolution beneath Sangeang Api volcano, East Sunda arc, Indonesia. J Petrol 44:491–515

Vila T, Sillitoe RH (1991) Gold-rich porphyry systems in the Maricunga belt, northern Chile. Econ Geol 86:1223–1238

Walker JA, Patino LC, Carr MJ, Feigenson MD (2001) Slab control over HFSE depletions in central Nicaragua. Earth Planet Sci Lett 192:533–543

Wang Q, McDermott F, Xu JF, Bellon H, Zhu YT (2005) Cenozoic K-rich adakitic volcanic rocks in the Hohxil area, northern Tibet: lower-crustal melting in an intracontinental setting. Geology 33:465–468

Wang Q, Wyman DA, Xu J-F, Zhao ZH, Jian P, Xiong XL, Bao Z-W, Li C-F, Bai Z-H (2006) Petrogenesis of Cretaceous adakitic and shoshonitic igneous rocks in the Luzong area, Anhui Province (eastern China): implications for geodynamics and Cu–Au mineralization. Lithos 89:424–446

White AJR, Chappell BW (1983) Granitoid types and their distribution in the Lachlan Fold Belt, southeastern Australia. In: Roddick JA (ed) Circum-Pacific Terranes. Geol Soc Am Mem 159:21–34

Wilson M (1989) Igneous petrogenesis: a global tectonic approach. Harper Collins Academic, p 466

Woodhead J, Eggins S, Gamble J (1993) High field strength and transition element systematics in island arc and back-arc basin basalts: evidence for multi-phase melt extraction and a depleted mantle wedge. Earth Planet Sci Lett 114:491–504

Xiao L, Clemens JD (2007) Origin of potassic (C-type) adakite magmas: experimental and field constraints. Lithos 95:399–414

Xiong XL, Li XH, Xu JF, Li WX, Zhao ZH, Wang Q (2003) Extremely high-Na adakite-like magmas derived from alkali-rich basaltic underplate: the Late Cretaceous Zhantang andesites in the Huichang Basin, SE China. Geochem J 37:233–252

Zhang Q, Wang Y, Qian Q (2001) The characteristics and tectonic-metallogenic significances of the Mesozoic adakites in eastern China. Acta Petrol Sin 17:236–244 (in Chinese with English abstract)